Inorg. Chem. **2008**, *47*, 8464−8472

Forum

$Ag_4V_2O_6F_2$ (SVOF): A High Silver Density Phase and Potential New Cathode Material for Implantable Cardioverter Defibrillators

Frédéric Sauvage,[†] Vincent Bodenez,[‡] Hervé Vezin,[§] Thomas A. Albrecht,[†] Jean-Marie Tarascon,[‡] and Kenneth R. Poeppelmeier*,[†]

Department of Chemistry, Northwestern University, Evanston, Illinois 60208, LRCS, CNRS UMR 6007, Université de Picardie Jules Verne, 33 rue St. Leu, 80039 Cedex, France, and LCOM, CNRS UMR 8009, Bat. C4, 59655 Villeneuve d'Ascq Cedex, France

Received April 30, 2008

The electrochemical reactivity of the cathode material $Ag_4V_2O_6F_2$ (SVOF) versus lithium, with a particular emphasis on the lithium insertion mechanism, was studied by means of the complementary techniques in situ X-ray diffraction, electron paramagnetic resonance, and high-resolution transmisssion electron microscopy. This study confirms the initial reports of a high capacity for SVOF of 148 mAh/g above 3 V and that the reduction of silver above 3 V (vs Li^+/Li^0) leads to a loss of SVOF crystallinity until it becomes completely amorphous between the third and fourth lithiums inserted. Next, vanadium is reduced between 2.5 and 1.5 V (vs Li^+/Li^0) for the fifth and sixth lithiums inserted. In addition, the polarization within the cathode is significantly lower for the vanadium reduction than for the silver reduction. The silver metal morphologies consisted of nanoparticles (∼5 nm diameter) and dendrites and were both seen in samples of lithiated SVOF.

Introduction

Inorganic chemistry plays an active role in many different fields of medicine. For example, inorganic chemists are involved in the development of electrochemical-based ion/molecular sensors to analyze and quantify in situ and/or in vivo vital signs. They also contribute to advances in the elaboration of biomaterial compatible glasses for bone grafting or, more generally, for restorative surgery. One significant step forward in the biomedical area that inorganic chemistry has made possible is the management of cardiac dysfunction including arrhythmia. Years of intensive research have led to small and more efficient batteries as the power source for implantable cardioverter defibrillators (ICDs). To meet the stringent requirements of high-energy output and reliability, the cathode material of the lithium primary battery is at the core of ICD research. Since 1984, $Ag_2V_4O_{11}$ (SVO) has provided the high chemical/electrochemical stability and high discharge rate required of the cathode material. To replace SVO, a new material would need to display a higher volumetric capacity and redox potential while maintaining the above-mentioned electrochemical characteristics.

ICDs enable the treatment of human ventricular fibrillation by administering either a 700−800 V shock to the right ventricle or a low-energy stimulus similar to a cardiac pacemaker. Since its invention more than 25 years ago, seven generations of power sources for ICDs have been subsequently reported.[1] The volumetric efficiency was improved between these designs and is considered more important than the gravimetric capacity in order that the device is of a reasonable size in the chest cavity. Two such improvements were the reduced headspace and separator volume. In addition, the transition from a two-cell to a single-cell battery was, from a technological point of view, a significant breakthrough in ICD size reduction. This device delivers therapy from a lithium primary battery supplying two parallel capacitors to drive high-voltage pulse discharges. These

* To whom correspondence should be addressed. E-mail: krp@northwestern.edu.
[†] Northwestern University.
[‡] LRCS, CNRS UMR 6007, Université de Picardie Jules Verne.
[§] LCOM, CNRS UMR 8009.

(1) Crespi, A. M.; Somdahl, S. K.; Schmidt, C. L.; Skarstad, P. M. *J. Power Sources* **2001**, *96*, 33–38.

10.1021/ic800793e CCC: $40.75
Published on Web 09/29/2008

capacitors are charged within a few seconds to administer eventual subsequent discharges.[2] For this reason, during the battery's discharge, the successive electrochemical steps necessitate high kinetics and good Li^+/e^- conduction to reduce battery polarization and to maintain efficient delivery of battery power. Meeting these requirements, the cathode SVO has been a commercial success because of its high chemical stability[3] and good electron/ion conductivity ($\sigma_{e^-} \sim 10^{-2}$ S/cm and $D_{Li^+} \sim 10^{-8}$ cm^2/s).[4,5] The electrode has been so carefully optimized that SVO provides a performance close to what can be theoretically expected. To realize additional size reduction and to achieve the next level in performance, new cathode materials exhibiting a higher volumetric capacity and a greater capacity above 3 V (vs Li^+/Li^0), while maintaining high electrode stability and discharge rates, will be required.

To address these issues, our approach is to synthesize new materials with significantly greater Ag/V ratios and partial fluoride substitution for oxide to increase the cell potential.[6] Our group reported recently the reactions of Ag_2O and V_2O_5 in HF(aq) under hydrothermal conditions.[7] This study established the preferred composition and relative solubilities that lead to the formation of red, transparent single crystals of the new silver vanadium oxyfluoride $Ag_4V_2O_6F_2$ (SVOF). Preliminary characterizational and electrochemical results, including a higher crystal structure density of 6.03 g/cm^3 (vs 4.80 g/cm^3 for SVO) and a higher capacity above 3 V (vs Li^+/Li^0), were encouraging.[6,8] From a capacity point of view, SVO can deliver approximately 100 mAh/g above 3 V, which is largely due to the reduction of silver; by comparison, the greater Ag/V ratio enables SVOF to exhibit a superior capacity of ca. 148 mAh/g through two biphasic transitions at around 3.40 and 3.20 V (vs Li^+/Li). It is also noteworthy, owing to its high density ($\rho = 6.03$ g/cm^3), that SVOF can provide almost twice the volumetric capacity above 3 V as compared to SVO, 892 mAh/cm^3 vs 479 mAh/cm^3, respectively.

In light of SVOF's potential as a new cathode for medical battery applications, we embarked on this collaboration to gather additional information on the electrochemical reactivity of SVOF versus lithium and the lithium insertion mechanism. To understand the aforementioned properties and processes, in situ X-ray diffraction (XRD) measurements during electrode reduction, as well as electron paramagnetic resonance (EPR) and high-resolution transmission electron microscopy (HRTEM) investigations, were pursued. The combined results will be discussed in this Forum Article and a mechanism proposed.

Experimental Section

SVOF Synthesis. $Ag_4V_2O_6F_2$ (SVOF) was synthesized successfully as a single phase from autogenous hydrothermal conditions.[6,7] The reactants consisting of 0.3972 g of Ag_2O, 0.0779 g of V_2O_5, and 0.2572 g of HF(aq) (48−50% by weight) corresponding to a 4:1 Ag/V molar ratio were combined within a FEP Teflon pouch.[9] The sealed pouch was then placed in a 125 mL PTFE Teflon-lined autoclave (Parr Instruments), which was backfilled with 42 mL of deionized H_2O. The autoclave was heated for 24 h at 150 °C and cooled at 0.1 °C/min to room temperature. Around 0.25 g of water from the backfill entered the pouch during the reaction owing to the semipermeability of the FEP Teflon to H_2O above 120 °C. Finally, the pouch was opened under air, and the products were filtered to retrieve red crystals of SVOF in 85% yield based on V.

Physical Characterization. The XRD patterns were recorded in a $\theta/2\theta$ configuration using a Bruker D8 diffractometer with Cu Kα radiation ($\lambda = 0.154\ 18$ nm). The particle size and morphology were investigated using an environmental scanning electron microscope FEI Quanta 200FEG coupled with an energy-dispersive X-ray spectroscopy (EDS) analysis system (Oxford Link Isis). To further investigate the local structure of the discharged material, HRTEM experiments were also performed using a FEI Tecnai F-20 S-twin microscope. For this, the battery was dismantled in an argon-filled glovebox and the retrieved cathode product was thoroughly washed three times in DMC before being deposited on a copper grid coated with a lacey-carbon film. A home-designed TEM sample holder, which allows the investigation of air sensitive materials, was used to prevent the discharged SVOF from further reaction or decomposition prior to the microscopy investigations.

EPR experiments were performed on different electrochemically lithiated SVOF materials (from $Li_0Ag_4V_2O_6F_2$ to $Li_{3.5}Ag_4V_2O_6F_2$) at room temperature and 4 K using a Bruker ELEXYS E580 X-band spectrometer with an amplitude modulation of 1 G and microwave power of 2 mW for continuous-wave (CW) experiments. To recover the partially lithiated material, the batteries were dismantled in an argon-filled glovebox and rinsed with DMC. The material was transferred to the EPR tube and sealed while in the glovebox and then flame-sealed under vacuum. The three-pulse electron spin-echo envelope modulation (ESEEM) experiment $\pi/2-\tau-\pi/2-T-\pi/2-\tau$ echo was performed with 16 ns $\pi/2$ pulse duration, and the time domain was recorded at $\tau + T$ and extracted from a Fourier transform. Experiments were recorded at various τ values to avoid the inherent "blind spots" in such a sequence.

As a complement to these techniques, in situ XRD experiments, recorded on a Bruker D8 diffractometer with a copper anticathode, were performed by utilizing an electrochemical cell capped by a beryllium window functioning as the positive-current collector. The electrochemistry of this cell was controlled by a Mac Pile galvanostat system, at a discharge rate of ca. D/10 (insertion of 1 Li^+ in 10 h), and XRD patterns were collected at intervals of 0.09 Li^+ per formula unit.

Electrochemical Tests. The electrochemical characterization of SVOF was carried out by manually grinding and mixing the single crystals with 14% by weight SP-type carbon black. The measurements were recorded following a two-electrode configuration using a Swagelok-type cell assembled in an argon-filled glovebox. Lithium metal foil was used as the counter and reference electrodes. Two pieces of Whatman GF/D borosilicate glass fiber sheets were thoroughly soaked with a 1 M $LiPF_6$ EC/DMC 1:1 electrolyte

(2) Gomadam, P. M.; Brown, J.; Scott, E. R.; Schmidt, C. L. 211th ECS Meeting, Chicago, IL, May 2006; Abstract 383.
(3) Takeuchi, K. J.; Marschilok, A. C.; Davis, S. M.; Leising, R. A.; Takeushi, E. S. *Coord. Chem. Rev.* **2001**, *219*, 283–310.
(4) Onoda, M.; Kanbe, K. *J. Phys.: Condens. Matter* **2001**, *13*, 6675–6685.
(5) Lee, J. W.; Popov, B. N. *J. Power Sources* **2006**, *161*, 565–572.
(6) Sorensen, E. M.; Izumi, H. K.; Vaughey, J. T.; Stern, C. L.; Poeppelmeier, K. R. *J. Am. Chem. Soc.* **2005**, *127*, 6347–6352.
(7) Albrecht, T. A.; Stern, C. L.; Poeppelmeier, K. R. *Inorg. Chem.* **2007**, *46*, 1704–1708.
(8) Izumi, H. K.; Sorensen, E. M.; Vaughey, J. T.; Poeppelmeier, K. R. U.S. Provisional Patent 60/606,475, Sept 1, 2004.
(9) Harrison, W. T. A.; Nenoff, T. M.; Gier, T. E.; Stucky, G. D. *Inorg. Chem.* **1993**, *32*, 2437–2441.

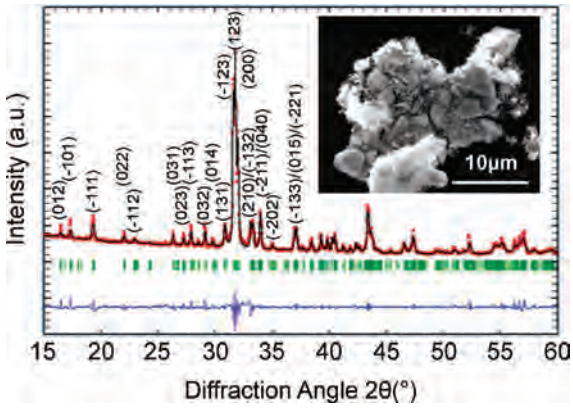

Figure 1. Full-pattern-matching refinement of the powder XRD pattern of ground SVOF. Inset: Scanning electron microscopy picture of the composite SVOF/C_{sp} electrode.

(LP30, Merck Selectipur grade). The electrode cycling tests were monitored by a VMP.

Results and Discussion

Characterization of SVOF. Following the synthetic route described in the Experimental Section, pure and well-crystallized SVOF is easily prepared (Figure 1). The unit cell parameters were refined using the reported monoclinic crystal structure and Fullprof software in full-pattern-matching mode.[10] The cell parameters thus obtained [a = 5.596(1) Å, b = 10.554(2) Å, c = 12.516(3) Å, and β = 90.464(6)°] were in agreement with those reported from the single-crystal structure determination. As a result of the grinding/mixing step with carbon, the needlelike single crystals of SVOF were broken into irregular pieces of heterogeneous size up to ~20 μm (Figure 1, inset). EDS acquisitions on different areas revealed the appropriate Ag/V = 2 ratio within the particles.

The SVOF structure is composed (Figure 2) of isolated chains of alternating corner-sharing VO_4F_2octahedra and VO_4 tetrahedra along the b axis. Between the (101) sheets of chains, silver cations are distributed among four distinct crystallographic sites where silver adopts 4-, 5-, or 7-fold coordination [$Ag(3)O_3F$, $Ag(1)O_4F$, $Ag(2)O_4F_3$, and $Ag(4)O_5F_2$]. Although the crystallographic directions [100] and [010] appear favorable for silver ion diffusion, the optimal diffusion pathways are not yet understood.

Electrochemical Properties. Figure 3a shows a typical discharge/charge trace of SVOF down to a cutoff potential of ca. 0.01 V (vs Li^+/Li^0). Despite a moderate cycling rate (i.e., C/10), the reaction of lithium with SVOF appears mostly irreversible, in contrast to SVO.[11−13] The entire discharge down to 0.01 V corresponds to the uptake of approximately 17.2 Li^+ per formula unit, or a gravimetric capacity of around 700 mAh/g (the capacity from C_{sp} is included in this value). Approximately half of this capacity is recovered during the subsequent charge. More insights on the electrochemical reversibility of the system are emphasized in Figure 3b. The cell recharge after two or four lithiums inserted, corresponding to a cutoff potential of 3.01 or 2.48 V (vs Li^+/Li^0), depicts a highly irreversible lithium reaction mechanism given that approximately 85% and 80% of the discharged capacity is not recovered, respectively. Lithium insertion into SVOF proceeds along two narrow plateaus above at ~3.45 and 3.25 V in OCV conditions,[6] followed by a smooth and continuous potential decrease reminiscent of solid solution behavior. In comparison to SVO, the increase of the silver reduction potential by about 300 mV is due to the presence of fluoride within the silver environment that modifies its chemical potential via a strengthening of the ionic character of the Ag−O/F bonds. The discharge trace of SVOF is compared in Figure 4a to SVO synthesized by a similar solvothermal route.[7] The SVO recovered from the hydrothermal synthesis formed needlelike, 2−5 μm long, 0.2−1 μm wide, and 50−100 nm thick particles. Further details on the characterization and electrochemical properties of SVO obtained

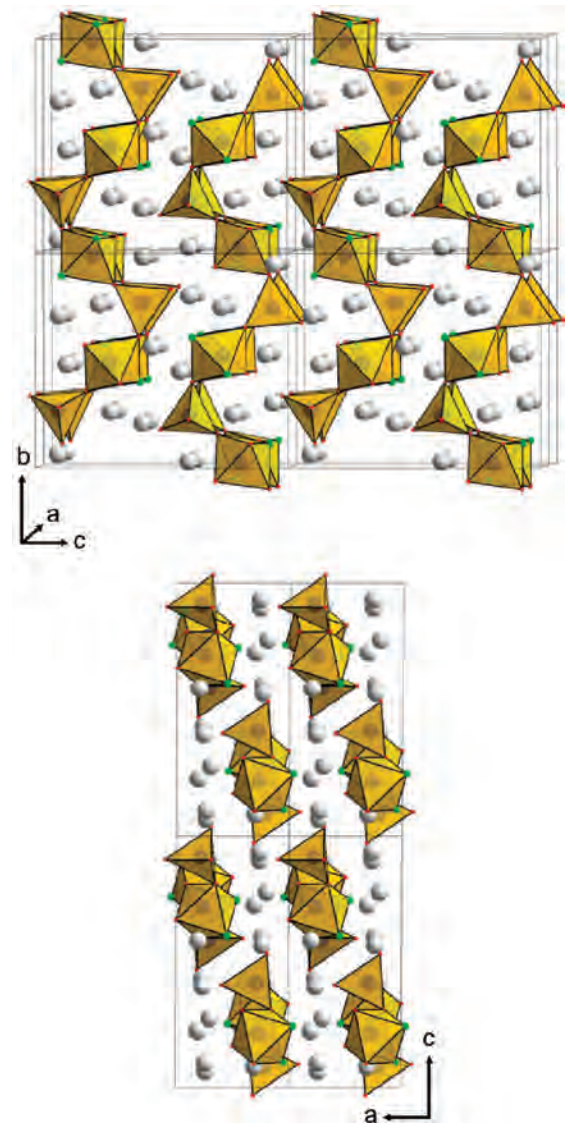

Figure 2. Structural representation of SVOF in the *bc* and *ac* planes with the V^{5+}-centered polyhedron.

(10) Roisnel, T.; Rodriguez-Carjaval, J. *Fullprof*, version Dec 2005; France, 2005.
(11) Garcia-Alvarado, F.; Tarascon, J.-M. *Solid State Ionics* **1994**, *73*, 247–254.
(12) West, K.; Crespi, A. M. *J. Power Sources* **1995**, *54*, 334–337.
(13) Kawakita, J.; Makino, K.; Katayama, Y.; Miura, T.; Kishi, T. *J. Power Sources* **1998**, *75*, 244–250.

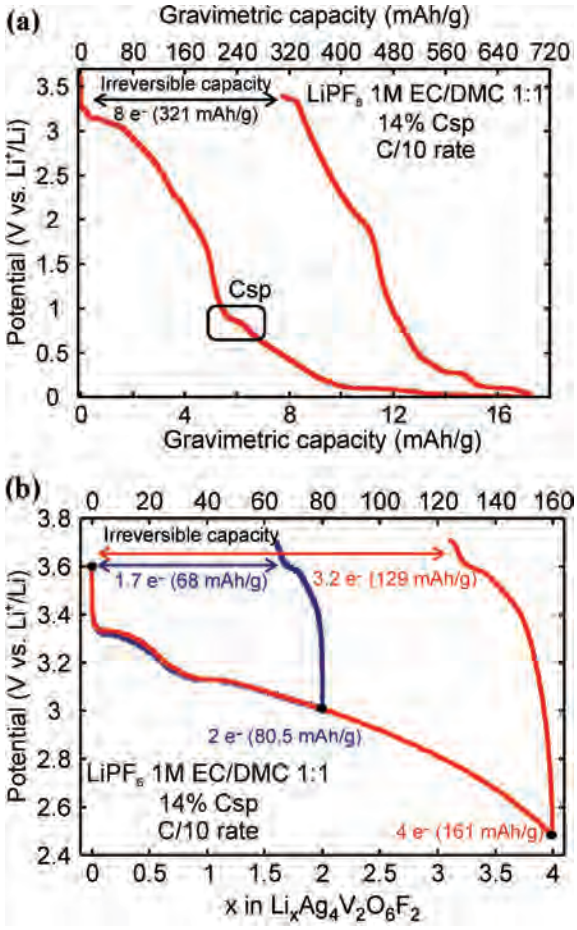

Figure 3. First cycle galvanostatic curve recorded at the C/10 rate of a composite SVOF/C_{sp} electrode in a 1 M $LiPF_6$ EC/DMC 1:1 electrolyte (a) down to a 0.01 V cutoff potential and (b) after two and four lithiums inserted.

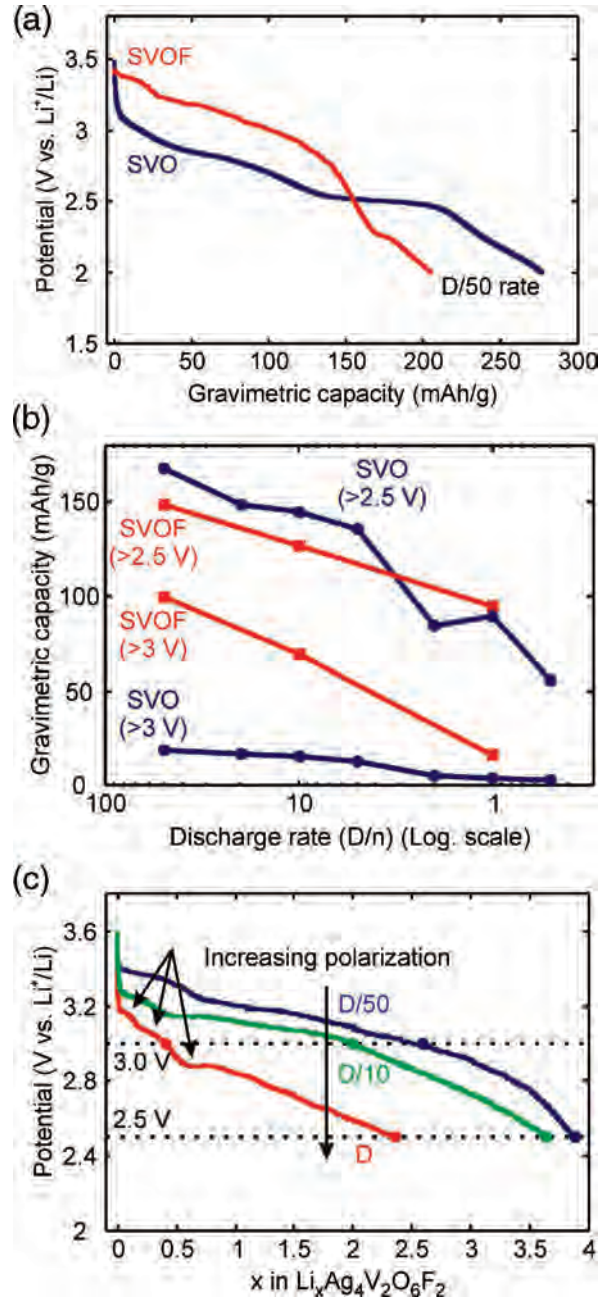

Figure 4. (a) Comparison of a galvanostatic-driven discharge performed at D/50 between SVOF and SVO synthesized by a similar solvothermal route. (b) Evolution of the electrode capacity as a function of the discharge rate beyond 3 and 2.5 V for SVOF and SVO. (c) Influence of the discharge rate on the electrochemical discharge curve of SVOF (D/50, D/10, and D).

by this route will be reported elsewhere. As mentioned, by discharging both cathodes at D/50, SVOF exhibits a significantly higher potential than SVO for the first 150 mAh/g, where a potential crossover between materials occurs. The benefit of SVOF above 3 and 2.5 V is shown in Figure 4b, where the influence of the discharge rate on the capacity of SVOF and the SVO is depicted. A decrease of the capacity with an increase in the discharge rate is noticed for SVOF and SVO. Such an influence of the discharge rate on the electrochemical capacity was reported for SVO prepared by a solid-state reaction.[14−16] While 148 mAh/g is thermodynamically available above 3 V for SVOF, 101 mAh/g is accessible at D/50, 80 mAh/g at D/10, and 16 mAh/g is recovered at D. At a cutoff potential of 2.5 V, a comparable capacity drop with the discharge rate is also observed (156, 147, and 95 mAh/g recorded at D/50, D/10, and D rates, respectively). Owing to the fact that both compounds exhibit the formation of silver metal, which increases the electronic conductivity of the composite electrode, such power rate limitations, which can translate to high polarization observed on the charge/discharge curves, are more prone to originate from the structure rather than from electronic limitations. Nevertheless, it is important not to overinterpret this comparison because the particle size, electrode porosity, etc., are parameters that can also affect the performance and rate capability of the electrode. A more extensive examination of the discharge curves at various rates reveals differences that suggest the lithium insertion and silver extraction are rather complex. In fact, a third feature appeared when the cell was more rapidly discharged at D, while such an additional plateau does not appear when the cell is discharged at D/50 (Figure 4c, arrows).

(14) Ramasamy, R. P.; Feger, C.; Strange, T.; Popov, B. N. *J. Appl. Electrochem.* **2006**, *36*, 487–497.
(15) Crespi, A. M.; Skarstad, P. M.; Zandbergen, H. W. *J. Power Sources* **1995**, *54*, 68–71.
(16) Beninati, S.; Fantuzzi, M.; Mastragostino, M.; Soavi, F. *J. Power Sources* **2006**, *157*, 483–487.

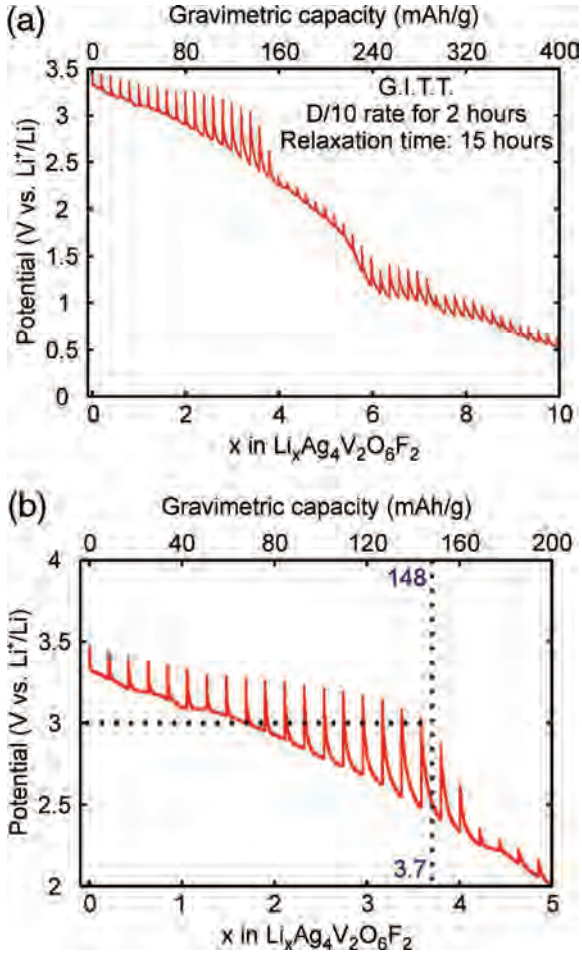

Figure 5. GITT curve of a SVOF/C_{sp} composite electrode in a 1 M $LiPF_6$ EC/DMC 1:1 electrolyte by applying a D/10 discharge rate for 2 h followed by 15 h of relaxation time for (a) 0–10 Li^+ and (b) 0–5 Li^+ showing the transition from the first to the second domain.

To evaluate the difference between the discharge curve and the open circuit potential of SVOF, galvanostatic intermittent titration technique (GITT) measurements were performed. For this, a cathodic current corresponding to an insertion rate of D/10 was applied for 2 h. This step was followed by a relaxation period ($I = 0$) of 15 h. Note the existence of a significant electrode polarization that increases from 275 to 550 mV during the uptake of the first 4 equivalents of lithium followed by an abrupt decrease near $x = 3.80$ to values less than 50 mV (Figure 5). The significant polarization change that occurs near $x = 4$ suggests a relationship between the amount of lithium reacted and the 4 equivalents of silver based on the formula $Ag_4V_2O_6F_2$. Upon further lithium insertion, two additional lithium composition domains appear that differ by the amplitude of their polarization, which implies different reactivity mechanisms. The second domain has a significantly lower polarization between the fourth and sixth lithiums inserted, followed by a third domain characterized by an increase in the polarization.

Lithium Reaction Mechanism. To understand the insertion mechanism that gives rise to these different phenomena, we embarked on an in situ XRD study. These measurements revealed the structural evolution of SVOF during lithium insertion. Figure 6a gathers the diffractograms recording each 0.09 Li^+ inserted within the lithium composition range $Li_0Ag_4V_2O_6F_2$ to $Li_1Ag_4V_2O_6F_2$. At the early stage of the lithium insertion, the progressive appearance of two diffraction peaks centered at $2\theta = 38.16°$ and 44.32° is assigned to silver metal. No perceptible shift of the SVOF diffraction peaks was noted. However, simultaneously, one can also notice a slight intensity decrease and broadening of the peaks corresponding to the lithiated SVOF phase, implying the onset of a structural amorphization or a decrease in crystallinity (Figure 6b). Such effects (increase in the silver content peak and decrease in the Li_xSVOF main peaks) become more pronounced upon further lithiation ($1 \leq x \leq 4$ in $Li_xAg_4V_2O_6F_2$), such that by $x = 4$ a composite electrode consisting of well-crystallized metallic silver coexists with an "X-ray" amorphous matrix. The mismatch between the ionic radii of lithium ($r_{Li^+} = 0.76$ Å) and silver ($r_{Ag^+} = 1.15-1.35$ Å) and the atomic radius of silver ($r_{Ag} = 1.44$ Å) is most likely at the origin of these structural changes.[17]

Further discharge, $4 \leq x \leq 7$ in $Li_xAg_4V_2O_6F_2$, does not noticeably modify the amplitude of the silver peak but leads to a full and complete amorphization of the SVOF phase (Figure 7a). There is also the peculiar appearance and disappearance of two unidentified broad diffraction peaks at $2\theta = 21.32°$ and 23.62° between the composition $Li_2Ag_4V_2O_6F_2$ and $Li_5Ag_4V_2O_6F_2$. Although their origin is not clear, we speculate that some structural correlation persists during the silver withdrawal. This feature is not reversible because we did not observe any phase recrystallization when recharging the cell. This experimental evidence demonstrates the irreversible character of the silver reduction, in contrast to the reported reversible copper extrusion mechanism in $Cu_{2.33}V_4O_{11}$.[18] Finally, at more reductive potentials, an alloying reaction involving the silver metal, still in electronic contact with the composite electrode, and the lithium is observed. The formation of $AgLi_x$ alloys was confirmed by XRD on the discharged SVOF with the occurrence of both AgLi and Ag_4Li_9 diffraction peaks, while concurrently the two silver metal peaks practically vanished (Figure 7b). The reactivity of silver metal versus lithium has been investigated by Taillades and Sarradin,[19] where both the reported diffraction evidence and the electrochemical signature at low potential (i.e., <1.5 V vs Li^+/Li^0) support the alloying reaction between silver and lithium on fully discharged SVOF.

The decreasing intensity of the SVOF diffraction peaks together with the appearance of the silver metal was followed by integration of the diffraction peak area of the silver (111) reflection as a function of the lithium content (Figure 8). A linear relationship was observed between the loss of crystallinity of SVOF and the amount of lithium inserted up to the point where the material becomes amorphous between $Li_3Ag_4V_2O_6F_2$ and $Li_4Ag_4V_2O_6F_2$. Interestingly, a nonlinear variation in the appearance of silver metal was observed and reaches its maximum near the composition $Li_4Ag_4V_2O_6F_2$.

(17) Shannon, R. D. *Acta Crystallogr.* **1976**, *A32*, 751.
(18) Morcrette, M.; Rozier, P.; Dupont, L.; Mugnier, E.; Sannier, L.; Galy, J.; Tarascon, J.-M. *Nat. Mater.* **2003**, *2*, 755.
(19) Taillades, G.; Sarradin, J. *J. Power Sources* **2004**, *125*, 199–205.

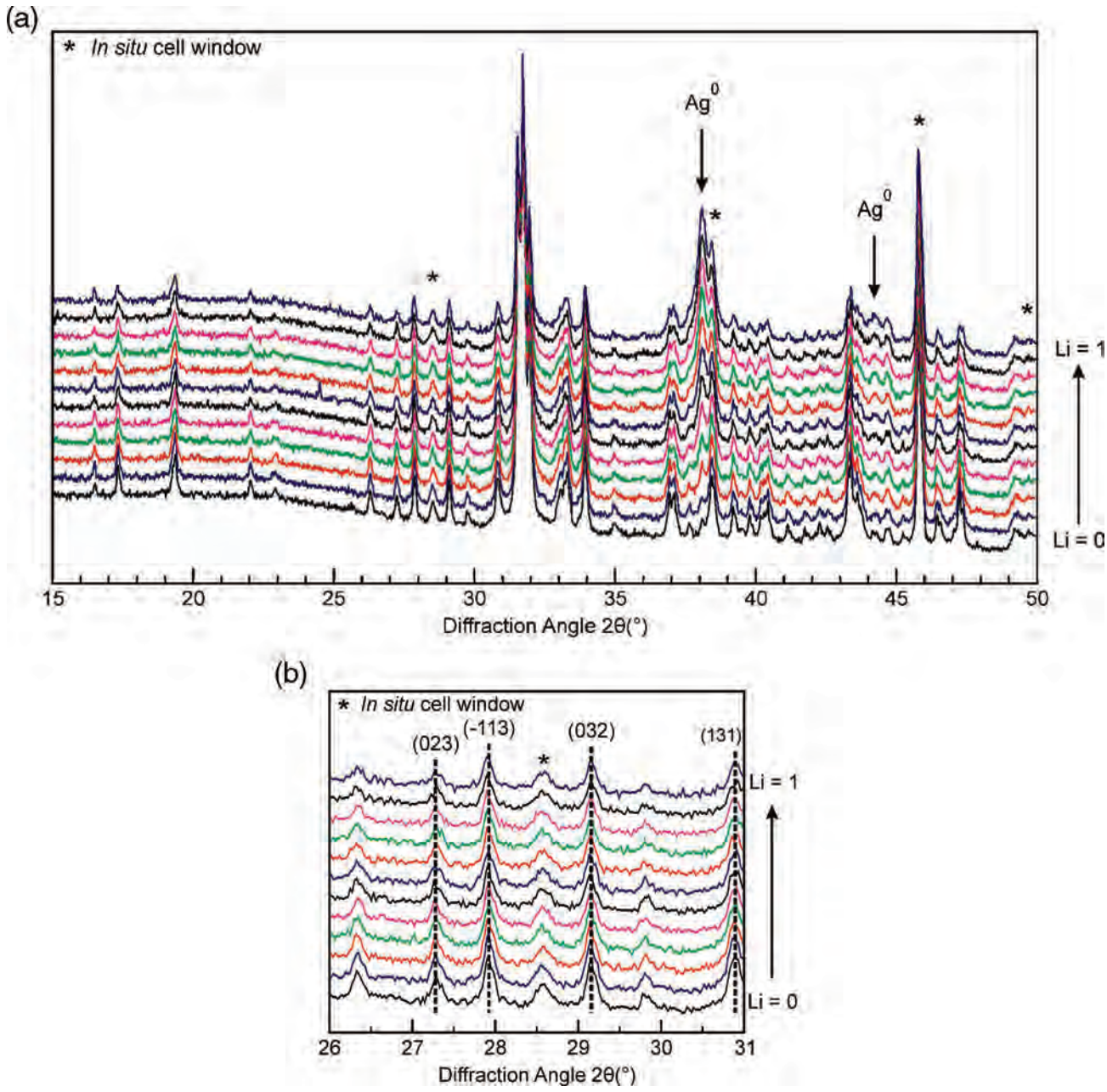

Figure 6. In situ evolution of the XRD pattern recorded every 0.09 Li^+ inserted at a D/10 discharge rate between $Li_0Ag_4V_2O_6F_2$ and $Li_1Ag_4V_2O_6F_2$ in 2θ ranges of (a) 15−50° and (b) 26−31°.

Such a deviation from linearity raised two hypotheses: (i) a competition between the Ag^+/Li^+ displacement reaction and V^{5+} reduction and (ii) the nucleation of nanocrystalline silver metal particles not detected by XRD.

To gain further insight into these subtle lithium-driven electrochemical reactions and to address the first hypothesis via the appearance of a V^{4+} signal, EPR measurements were performed on several electrochemically lithiated SVOF compositions between $Li_0Ag_4V_2O_6F_2$ and $Li_6Ag_4V_2O_6F_2$. The spectra recorded at room temperature, displayed in Figure 9, clearly evidenced no V^{4+} formation through this composition range. In addition, no V^{4+} feature was found by measurements at 4 K. The starting material, i.e., $Li_0Ag_4V_2O_6F_2$, exhibits a very weak EPR signal that may be due to a small concentration of paramagnetic defects. All of the spectra recorded by variation of the Li^+ amount from 1 to 6 consisted of a narrow isotropic line of 13 G at a g value of 2.0021. Moreover, we can clearly see that increasing the Li^+ inserted results in an increase of the EPR signal. Such a value of $g = 2.0021$, close to that of the free electron, has been reported to be related to the formation of Ag^0 nanoclusters and their surface conduction electrons.[20] Hence, the first 3.5 Li^+ reduce Ag^+, which allows us to rule out the first hypothesis. Furthermore, increasing the Li amount to Li_6 does not appear to result in the formation of V^{4+} species, suggesting that the composition range of 4−6 Li^+ corresponds to selective redox processes involving reduction of half of the V^{5+} species in SVOF (redox couple V^{5+}/V^{3+}) rather than all of the V^{5+} reduced to V^{4+}. This may reflect that the tetrahedral VO_4 groups in the isolated

(20) Bharathi Mohan, D.; Sunandana, C. S. *J. Phys. Chem. B* **2006**, *110*, 4569–4575.

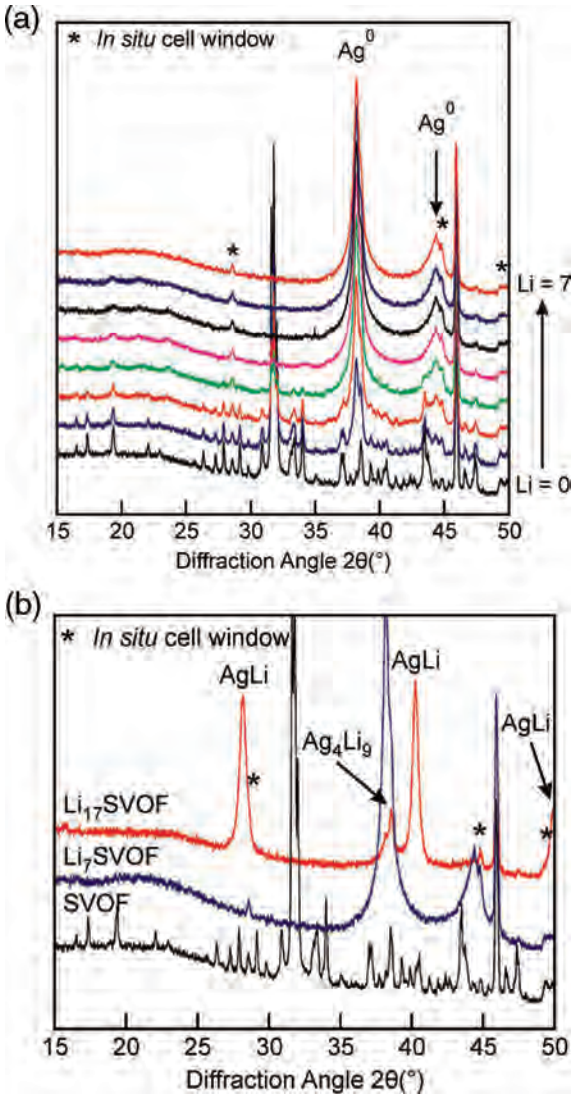

Figure 7. (a) In situ evolution of the XRD pattern recording every 1 Li^+ inserted at a D/10 discharge rate between $Li_0Ag_4V_2O_6F_2$ and $Li_7Ag_4V_2O_6F_2$ in a 2θ range of 15−50°. (b) Comparison of the XRD patterns for SVOF, $Li_7Ag_4V_2O_6F_2$, and $Li_{17}Ag_4V_2O_6F_2$.

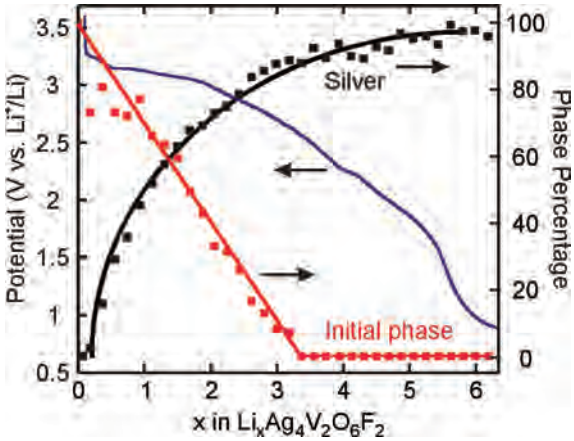

Figure 8. Evolution of the silver metal and SVOF XRD peak area as a function of x in $Li_xAg_4V_2O_6F_2$.

chains of alternating VO_4F_2 octahedra and VO_4 tetrahedra are difficult to reduce.[21] Although not common, a two-electron reduction of an oxide cathode material has been observed.[22]

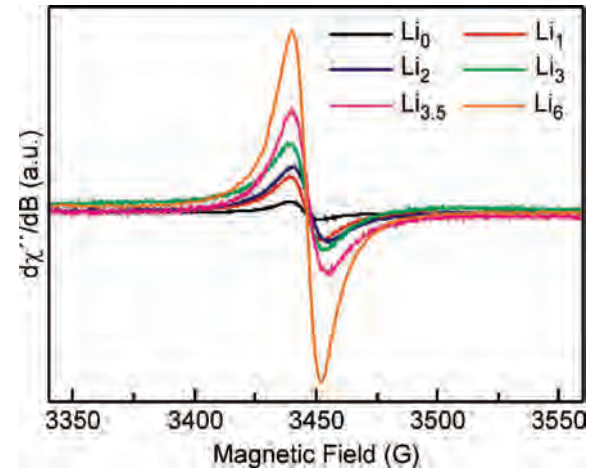

Figure 9. CW EPR spectra for $Li_xAg_4V_2O_6F_2$ for $x = 0-3$, 3.5, and 6. The spectra were recorded at room temperature.

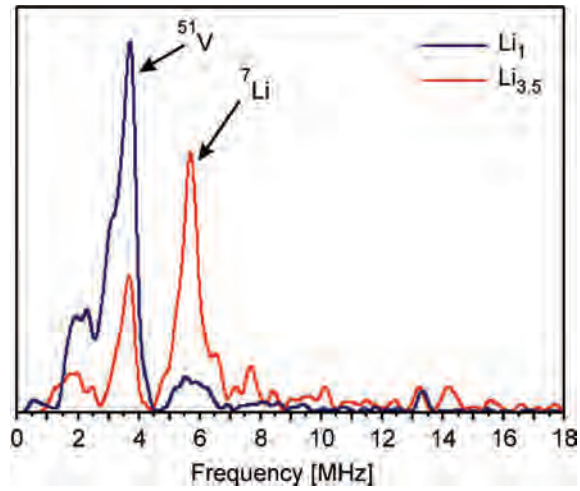

Figure 10. Three-pulse ESEEM spectra recorded at 4 K for $Li_1Ag_4V_2O_6F_2$ and $Li_{3.5}Ag_4V_2O_6F_2$.

In order to have a better understanding of the nuclear environment of these Ag^0 nanoclusters, three-pulse ESEEM experiments were also performed on samples lithiated to Li of 1 and 3.5. The spectra, Figure 10, were recorded using a τ value of 136 ns, which minimizes the "blind spots" effect. These show for 1 Li^+ insertion two peaks arising from the ^{51}V nuclear Larmor frequency detected at 3.9 MHz and the ^7Li nuclear frequency at 5.8 MHz. Increasing the Li^+ content from 1 to 3.5 results in a decrease of the ^{51}V peak and an increase of the ^7Li peak, which appears to indicate that the conduction electrons on silver are located closer to the lithium than the vanadium. For a value of Li^+ of 6, no pulsed EPR spectra can be measured at low temperature. Because the sample at 6 Li^+ is diamagnetic at low temperature, no spin echo can be recorded. Thus, we recorded a series of CW EPR spectra in the temperature range 4−45 K and found that the $g \approx 2$ signal decreased with decreasing temperature. This phenomenon comes from the J coupling constant owing to the exchange interaction mechanism between coupled

(21) Whittingham, M. S.; Zavalij, P. Y. *Int. J. Inorg. Mater.* **2001**, *3*, 1231–1236.
(22) Johnson, C. S.; Kim, J.-S.; Kropf, A. J.; Kahaian, A. J.; Vaughey, J. T.; Fransson, L. M. L.; Edström, K.; Thackeray, M. M. *Chem. Mater.* **2003**, *15*, 2313–2322.

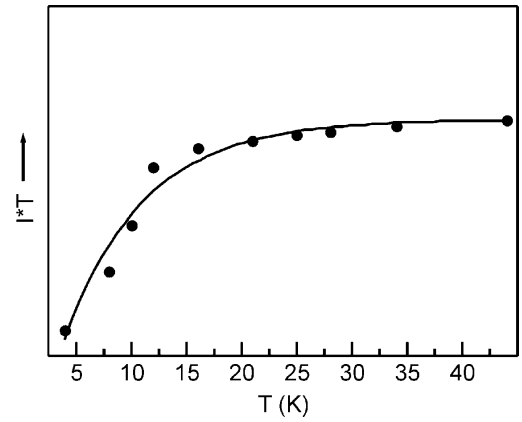

Figure 11. Plot of the EPR intensity signal × temperature product (*IT*) versus temperature for the $Li_6Ag_4V_2O_6F_2$ compound. The data were fitted according to the Bleaney−Bowers equation.

electronic spins. At low temperature, a populated diamagnetic $S = 0$ indicates an antiferromagnetic coupling between conduction electrons associated with the silver particles. Figure 11 shows the temperature behavior for the sample at 6 Li^+. When the product of the signal intensity and the temperature versus temperature is plotted, the *J* coupling constant can be fit according to the Bleaney−Bowers equation.[23] A *J* value of -4.2 cm^{-1} provides a satisfactory fit of the curve.

In light of the combined results provided by the in situ XRD investigation and the EPR, the three different domains pointed out by the GITT curve can be described by the sequence of (i) the silver displacement reaction with lithium, (ii) half of V^{5+} reduction to V^{3+}, and (iii) complete reduction to V^{3+} and the eventual formation of an Ag/Li alloy. Therefore, the significant drop in polarization observed around the fourth lithium inserted is due to a change from the Ag^+/Li^+ displacement reaction to an insertion redox reaction involving the reduction of V^{5+} and the insertion of lithium ion into the structure.

To investigate the second hypothesis, HRTEM was used to study the morphology of the formed silver metal on a sample that was electrochemically discharged at D/10 to 1.5 V. The bright-field images show the occurrence of two contrasts within the particles (Figure 12a). EDS and TEM measurements carried out on these two areas revealed the coexistence of silver metal (dark zone) within a matrix of composition $Ag_{0.12}-Li_x-V_2-O_y-F_z$ (Li_xSVOF). The small amount of unreduced silver in the Li_xSVOF matrix is consistent with the change in the GITT curve at $x = 3.8$ assigned to the end of the silver reduction. The unreduced silver could be isolated in the collapsed Li_xSVOF matrix and therefore very difficult to access for reduction. This explanation may also account for the continuous increase of the polarization between $x = 0$ and 3.8.

In addition to the formation of silver between the Li_xSVOF layers in the form of long submicron wide dendrites and particle exfoliation (Figure 12a, inset), the second morphology consists of silver metal nanoparticles of about 3−5 nm diameter within the Li_xSVOF matrix (Figure 12b). The observation of nanosized silver metal particles accounts for the discrepancy observed in the Bragg peak intensities in

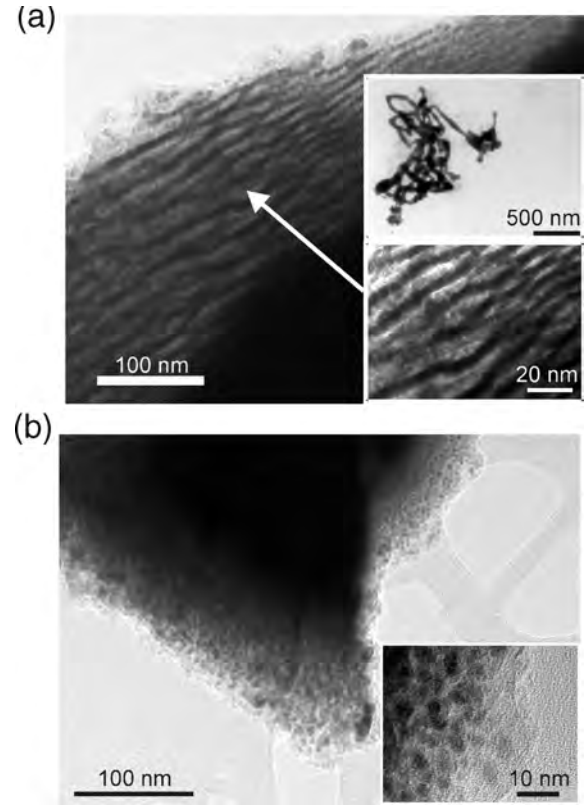

Figure 12. HRTEM bright-field image obtained on an electrochemically discharged SVOF showing (a) the particle exfoliation with silver dendrites and (b) the silver nanoparticles embedded in the amorphous Li_xSVOF matrix.

Figure 8 and also accounts for the broad silver diffraction peaks. The formation of two different silver morphologies may have their origin in the surfaces created during the grinding of the as-prepared SVOF crystallites. However, the coexistence of silver nanoparticles and silver dendrites also results from the influence of the discharge rate. Additional HRTEM investigations were performed on SVOF samples that were separately discharged at rates of D and D/50 to the same cutoff potential. Although both silver morphologies were still observed, the faster discharge rate surprisingly promotes the formation of silver dendrites. A similar relationship was reported for copper extrusion from the thiospinel $CuCr_2S_4$.[24] To account for this observation, we consider that the nanosized silver particles could originate from different pathways made favorable because of the low rate.

Conclusion

Additional galvanostatic and GITT electrochemical investigations have increased our understanding of the reactivity of $Ag_4V_2O_6F_2$ (SVOF) versus lithium. In situ XRD measurements combined with EPR investigations suggest that a Ag^+/Li^+ displacement reaction occurs from $Li_0Ag_4V_2O_6F_2$ to $Li_{\sim 4.0}Ag_4V_2O_6F_2$. This reduction is accompanied by (i) a

(23) Bleaney, B.; Bowers, D. K. *Proc. R. Soc. London A* **1952**, *214* (1119), 451–465.
(24) Bodenez, V.; Dupont, L.; Laffont, L.; Armstrong, A. R.; Shaju, K. M.; Bruce, P. G.; Tarascon, J.-M. *J. Mater. Chem.* **2007**, *30*, 3238–3247.

significant electrode polarization underscoring the difficulties of silver withdrawal and (ii) a continuous structure amorphization. This silver extrusion was found to be almost entirely irreversible. The metallic silver that forms exhibits two distinct morphologies: long dendrites with particle exfoliation and nanosized particles embedded in a Li_xSVOF matrix. As deduced by different EDS experiments, the amorphous matrix contains a small percentage of unreduced silver ions leading to an average composition $Ag_{0.12}Li_xV_4O_yF_z$. Following the silver displacement, a decrease in the cathode polarization is observed. This decrease is linked to a reversible vanadium redox of V^{5+} to V^{3+} present in the amorphous matrix. In order to minimize the polarization for high-rate silver-based electrodes, an engineered approach that decreases the length scale for ion diffusion by combining design of the particle size and microstructure is under study.

Acknowledgment. The authors gratefully acknowledge Prof. Loic Dupont for discussions on HRTEM. This work was supported by the National Science Foundation (Solid State Chemistry Awards No. DMR-0604454) and the Office of Naval Research (MURI Grant N00014-07-1-0620), and use of the Central Facilities was supported by the MRSEC program of the National Science Foundation (Grant DMR-0520513). V.B. is indebted to the Conseil Regional de Picardie for financial support.

IC800793E